J Mater Sci (2011) 46:7423–7430
DOI 10.1007/s10853-011-5705-3

Characterization of poly(ethylene-*co*-vinyl acetate-*co*-carbon monoxide)/layered silicate clay hybrids obtained by melt mixing

S. Anandhan · Harsha G. Patil · R. Rajesh Babu

Received: 4 March 2011 / Accepted: 8 June 2011 / Published online: 21 June 2011

Abstract In recent times, polymer-layered silicate nanocomposites have drawn a great deal of attention because they often exhibit tremendous improvements in material properties compared with virgin polymers or conventional micro- or macro-composites. In the present study, nanocomposites were developed from organically modified clay and poly(ethylene-*co*-vinyl acetate-*co*-carbon monoxide) by melt mixing. FTIR spectroscopy reveals that the interaction between the organoclay and EVACO is thermodynamically favored. High resolution wide angle X-ray diffraction and transmission electron microscopy were used to study the morphology of the nanocomposites. Elemental mapping by scanning electron microscopy indicates good dispersion and distribution of the nanoclay in EVACO matrix. The mechanical properties of the nanocomposites are optimum at a clay loading of 3%.

Abbreviations

PLS	Polymer layered silicate
EVACO	poly(ethylene-*co*-vinyl acetate-*co*-carbon monoxide)
FTIR	Fourier transform infra red
WAXD	Wide angle X-ray diffraction
TEM	Transmission electron microscopy
SEM	Scanning electron microscopy
O-MMT	Organically modified montmorillonite
DSC	Differential scanning calorimeter

S. Anandhan (✉) · H. G. Patil
Department of Metallurgical and Materials Engineering, National Institute of Technology-Karnataka, Surathkal, Mangalore 575025, Karnataka, India
e-mail: anandtmg@gmail.com; anandhan@nitk.ac.in

R. R. Babu
Department of Polymer Processing, Leibniz-Institut für Polymerforschung Dresden e. V., Hohe Strasse 6, Dresden 01069, Germany

Introduction

In the recent past, materials and structures showing geometric dimensions below 100 nm have gained a lot of attraction and stimulated research interest, even on some fancy ideas like molecular manufacturing or space elevators as well as on serious products for consumer goods, health, medical or food technology [1–5]. Nanocomposites are composites in which at least one of the phases shows dimensions in the nanometer range (1 nm = 10^{-9} m). They are reported to be the materials of twenty-first century in the view of possessing design uniqueness and property combinations that are not found in conventional composites. Polymer nanocomposites based on PLS hybrids have drawn a great deal of attention because they often exhibit tremendous improvements in material properties compared to either virgin polymers or conventional micro- or macro-composites [6–8]. The main reason for the remarkable improvements observed in PLS nanocomposites is the stronger interfacial interaction between the matrix and the silicate, compared to conventional filler-reinforced systems [9].

Nanoclays are clay minerals optimized for use in clay nanocomposites—multi-functional material systems with several property enhancements targeted for a particular application. Polymer–clay nanocomposites are an especially well-researched class of such materials. Nanoclays are a broad class of naturally occurring inorganic minerals, of which plate-like montmorillonite (MMT) is the most commonly used in materials applications. The MMT consists of ~1-nm-thick aluminosilicate layers

surface-substituted with metal cations and stacked in ~10-μm-sized multilayer stacks. The stacks can be dispersed in a polymer matrix to form polymer–clay nanocomposite. Within the nanocomposite, individual nm-thick clay layers are fully separated to form plate-like nanoparticles of very high aspect ratio. Even at low nanoclay loading, the entire nanocomposite consists of interfacial polymer, with majority of polymer chains residing in close contact with the clay surface. This can dramatically alter properties of a nanocomposite compared to the pure polymer. Potential benefits include increased mechanical strength, decreased gas permeability, superior flame-resistance, and even enhanced transparency when dispersed nanoclay plates suppress polymer crystallization [10–13].

The MMT based clays have been used for the preparation of the nanocomposites in the present study. MMT is a naturally occurring 2:1 phyllosilicate, which has the same layered and crystalline structure as talc and mica but a different layer charge [14]. The MMT crystal lattice consists of 1 nm thin layers, with a central octahedral sheet of alumina fused between two external silica tetrahedral sheets (in such a way, so that the oxygens from the octahedral sheet also belong to the silica tetrahedral). These layers organize themselves in a parallel fashion to form stacks with a regular van der Walls gap in between them, called interlayer or gallery. The Na^+ or Ca^{2+} ions residing in the interlayers could be replaced by organic cations such as alkyl ammonium ions or phosphonium ions by an ion-exchange reaction to render the hydrophilic layered silicate organophilic, so that polymer chains could be intercalated, thus causing the clay layer to be either swollen or exfoliated [15].

Although the intercalation chemistry of polymers toward layered silicates has long been known [16, 17], the field of PLS nanocomposites has recently gained impressive attention, due mainly to two important findings. First, the results obtained on Nylon-6/MMT nanocomposites showed that a small concentration of layered silicates led to remarkable changes in thermal and mechanical properties [6]. Second, Vaia et al. [18] observed that it is possible to melt-mix polymers with layered silicates, without the use of organic solvents.

Two particular characteristics of layered silicates are generally considered for PLS nanocomposites. The first is the ability of the silicate particles to disperse into individual layers (totally delaminated or exfoliated). The second is the ability to fine-tune their surface chemistry through ion exchange reactions with organic and inorganic cations. These two are, of course, interrelated, since the degree of dispersion of a layered silicate in a particular polymer matrix depends on the interlayer ionic species.

A novel polymeric material, poly(ethylene-*co*-vinyl acetate-*co*-carbon monoxide) (EVACO), which is a random terpolymer with carbonyl groups in the backbone has been used in the present study [19, 20]. EVACO is less crystalline compared with polyethylene because of the presence of bulky vinyl acetate groups in it. The polar acetate and carbonyl groups also help in producing good adhesion of EVACO with polar substrates like metals. The predecessor of EVACO, ethylene vinyl acetate (EVA) copolymer has been widely used in packaging applications because of its high level of transparency and good barrier properties. The presence of carbon monoxide in the form of carbonyl group makes EVACO not only photodegradable, but, also enhances its adhesion properties.

From the literature review, it has been found that there have been only a few reports on polymer systems based on EVACO. EVACO has been used as a photoreceptor medium [21], adhesive formulations [22], phase compatibilizer in polymer blends [23], and plasticizer for PVC [24]. Commercially EVACO has been used as an adhesion promoter in paints/coatings. To the best of the authors' knowledge, so far no attempt has been made to develop nanocomposites from EVACO as such.

In the present study, nanocomposites were developed from EVACO and an organically modified MMT by melt-blending technique and the structure–property relationship of the EVACO/O–MMT hybrids has been discussed.

Experimental

Materials

The details of the materials used in this study are given in Table 1.

Preparation of nanocomposites

The nanocomposites containing 1, 3, and 5% of the organoclay on w/w basis (samples designated as MM1, MM3, and MM5, respectively,) were prepared by melt mixing in a Haake Rheomix 600 internal mixer, having a mixing chamber volume of 65 cm^3, at a rotor speed of 60 rpm at 80 °C. Accurately weighed polymer and organoclay were taken in the mixing chamber, and the mixing was continued until the torque became stabilized. Torque versus time graphs (Fig. 1) were recorded during mixing. Immediately after mixing, the mixed mass was passed through a cold two-roll mill. The sheets were cut and remixed in the Haake Rheomix for further 2 min. The sheets were compression molded (Moore press, Birmingham, UK) in a frame and plate mold at 100 °C under a pressure of 5 MPa for 2 min. The sheets were removed from the mold after cooling the mold to room temperature under water circulation.

Table 1 Details of materials

Material	Supplier
Poly(ethylene-*co*-vinyl acetate-*co*-carbon monoxide)	Sigma-Aldrich Ltd, USA
(Elvaloy® 4924 from Du Pont, USA)	
Composition	
Carbon monoxide—10 wt%	
Vinyl acetate—24 wt%	
Ethylene—66 wt%	
Properties	
Weight average molecular weight $M_w > 250{,}000$	
Melt index (190 °C/2.1 kg) 35 g 10 min^{-1}	
Hardness (shore A, 10 s ASTM D 2240-81) 70	
Modified montmorillonite	Sigma-Aldrich Ltd, USA
(Nanomer® I.31PS from Nanocor Corporation, USA)	
Modifier	
15–35 wt% of octadecyl amine and	
0.5–5 wt% of aminopropyltriethoxysilane	

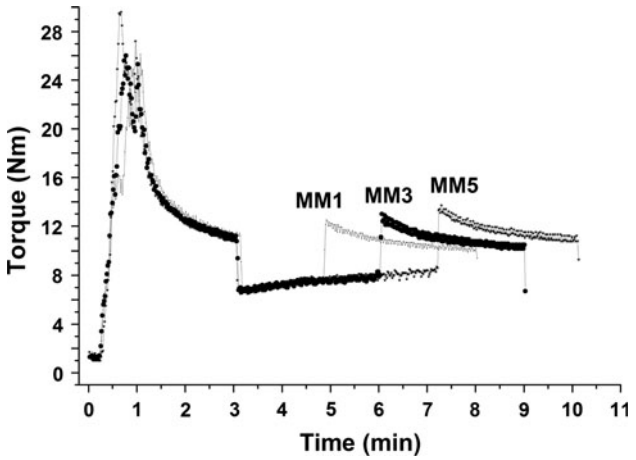

Fig. 1 Torque versus time curves for the melt mixing of O-MMT with EVACO

Characterization of nanocomposites

X-ray diffraction (XRD) analysis

High-resolution wide angle XRD spectra of the O-MMT and nanocomposites were recorded from 2° to 10° with a diffractometer (PANalytical high resolution XRD-I, PW 3040/60) using CuK_α ($\lambda = 1.542$ Å) at an accelerating voltage of 40 kV.

Transmission electron microscopy

TEM studies of the representative samples were carried out using a Philips transmission electron microscope (Tokyo, Japan) at an accelerating voltage of 75 kV. The ultrathin sections, about 50 nm thick, were prepared by cryomicrotoming in an RMC ultracryomicrotome (Tokyo, Japan) with glass knives (made with an RMC knife maker) after freezing the specimens below their glass-transition temperature (at −50 °C) with liquid nitrogen. The cryomicrotomed sections were deposited onto 400-mesh copper grids and were dried in a vacuum oven at 80 °C before TEM analysis.

Scanning electron microscopy

In order to assess the evenness of dispersion of dispersion of O-MMT in EVACO matrix, elemental mapping of the nanocomposites was carried out in a JEOL JSM-6380LA scanning electron microscope. The sample surfaces were sputtered with platinum in a sputtering unit (JEOL JFC 1600), auto fine coater, to make them conductive.

FTIR spectroscopy

The FTIR spectra of O-MMT, pristine EVACO, and a representative nanocomposite were recorded in a Shimadzu-IR Affinity-I FTIR spectrophotometer in transmission mode. To obtain the vibrational spectrum of O-MMT, it was mixed with spectral grade KBr and pressed into a thin wafer in a hydraulic press. For obtaining the spectra of neat EVACO and nanocomposite, their respective molded sheets were used. The samples were scanned from 4000 to 400 cm^{-1} with a resolution of 2 cm^{-1}, and 32 scans were averaged out for each spectrum.

Differential scanning calorimetry

DSC measurements were carried out in a Shimadzu DSC-60 differential scanning calorimeter. Typically, a sample of about 10 mg was heated first under a nitrogen atmosphere

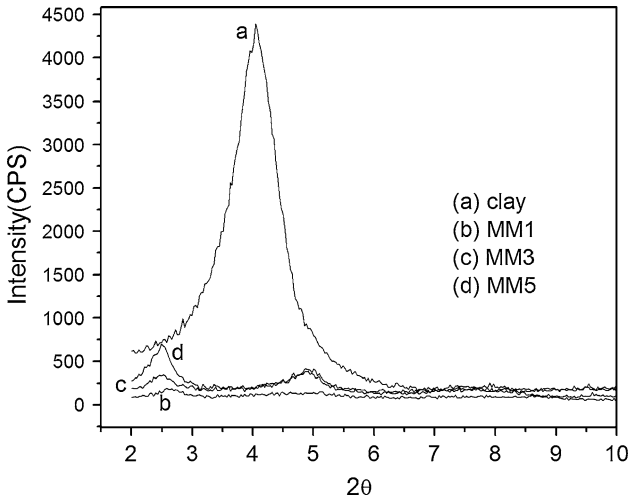

Fig. 2 HRXRD results of O-MMT and EVACO/O-MMT hybrids

Table 2 Interlayer spacing in the EVACO/organoclay hybrids

Sample type	2θ (°)	'd' spacing (nm)	Morphology
O-MMT	4.03	2.05	_
MM1	_	_	Exfoliation
MM3	2.5	3.52	Intercalation
MM5	2.5	3.52	Intercalation

(flow rate 50 mL min^{-1}) from −50 to 80 °C at a heating rate of 10 °C min^{-1} to relieve any thermal history of the glassy state. Then, the sample was allowed to cool down to −50 °C and was subsequently reheated from −50 to 80 °C. Heating was repeated at the same rate. The data obtained from the second scan were used for the determination of T_g of the neat polymer and the hybrids.

Mechanical properties

Dumb-bell specimens of the control and hybrid samples were punched out using an ASTM-C die from the molded sheets, and the testing was done according to ASTM D418-98A using a universal testing machine (Hounsfield H10KS) at a constant cross-head speed of 500 mm min^{-1}. Five specimens were tested for each type of sample, and the average values of the readings are reported.

Results and discussion

Morphology of the nanocomposites

HRXRD studies

XRD provides information on the changes of the interlayer spacing of the O-MMT upon the formation of a nanocomposite. The formation of an intercalated structure should result in a decrease in 2θ, indicating an increase in the d-spacing; the formation of an exfoliated structure usually results in the complete loss of registry between the

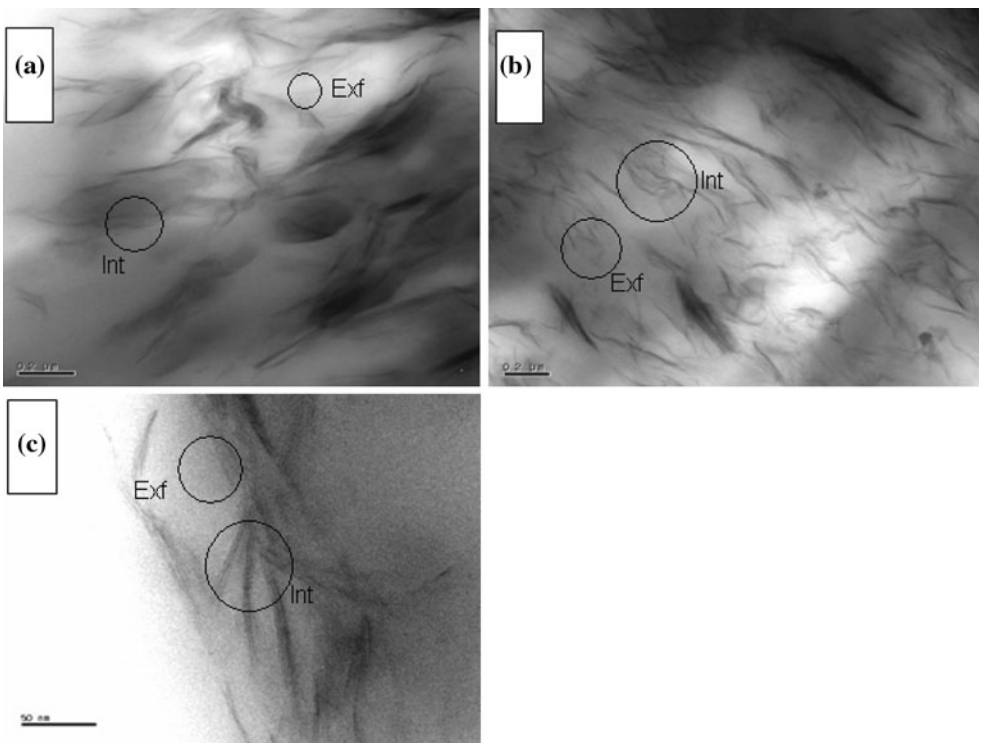

Fig. 3 TEM micrographs of O-MMT/EVACO hybrids. **a** MM1, **b** MM3, and **c** MM5

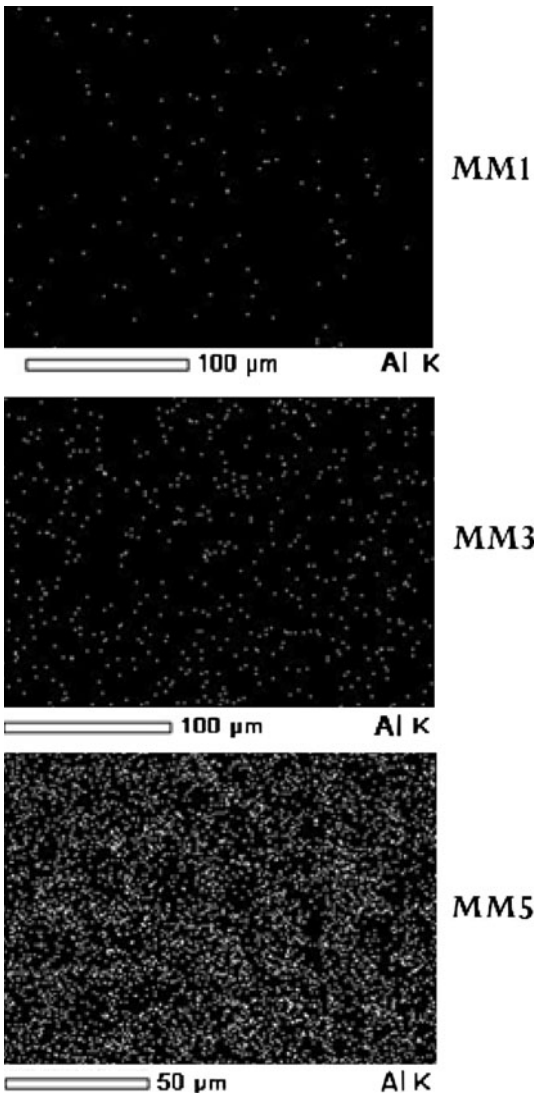

Fig. 4 Elemental mapping by EDX of O-MMT/EVACO hybrids

clay layers, and no peak can be seen in the XRD trace. In some cases, a disordered immiscible system is obtained, and this also shows no peaks, and so the absence of an XRD peak cannot be taken as definitive evidence for the formation of an exfoliated nanocomposite and additional evidence, usually TEM, is required. The XRD results give useful information on the state of organoclay in the polymer but do not provide a complete picture of the morphology. TEM is required to complement this information to enable the evaluation of the dispersion of O-MMT in the polymer matrix.

The XRD results are shown in Fig. 2. The interlayer spacing of the O-MMT has been calculated using Bragg's equation [6, 7, 10, 11] and the values are shown in Table 2. The XRD profile of MM1 has no peaks, indicating an exfoliated morphology of the O-MMT in the nanocomposite. MM3 and MM5 exhibit two peaks each, corresponding to their (001) and (002) planes in their respective XRD profiles indicating an expansion of the gallery gap. This suggests that the melt-mixing process has provided sufficient shear forces for the intercalation of the clay galleries by the polymer chains. At a lower clay loading (1 wt%), the shear forces are sufficient to cause predominant delamination of the clay layers.

TEM studies

The representative TEM micrographs of EVACO/O-MMT hybrids are shown in Fig. 3 (intercalated and exfoliated structures have been highlighted). The hybrid with 1 wt% clay exhibits a predominantly exfoliated morphology, whereas the hybrid with 3 wt% clay exhibits a mixture of intercalated and exfoliated morphologies (Fig. 3a, b). The TEM micrograph of the hybrid with 5 wt% of clay shows predominantly intercalated morphology (Fig. 3c). It is interesting to compare these results with those of the XRD results. While TEM clearly demonstrates the existence of a mixture of intercalated and exfoliated morphologies at all clay loading, XRD results provide a clear picture as to which type of morphology is predominant.

SEM studies

An optimum level of dispersion and distribution of nanoclay in a polymer matrix is necessary so as to achieve an improvement of mechanical, barrier, and thermal properties. The elemental mapping results obtained by energy dispersive X-ray analysis (EDX) indicate good dispersion and distribution of O-MMT in the EVACO matrix (Fig. 4), which in turn has caused improvement in the mechanical properties as discussed later.

FTIR spectroscopy

FTIR spectrum of the O-MMT is shown in Fig. 5, and the bands are assigned to the vibrations of various groups [25, 26] present in the O-MMT (Table 3). The FTIR spectra of pristine EVACO and MM5 are shown in Fig. 6.

To understand the chemical interaction between EVACO and O-MMT, Fowkes' equation was employed. Fowkes' equation relates change in IR peak position with enthalpy of interaction between the phases in a binary polymer system such as a blend or composite [27, 28]. Fowkes' equation is

$$\Delta H = 0.236 \times \Delta\bar{\nu} \quad (1)$$

where, ΔH is enthalpy of interaction between the phases in the binary polymer system, and $\Delta\bar{\nu}$ is shift in peak position (corresponding to a functional group of the polymer that is involved in interactions such as H-bonding).

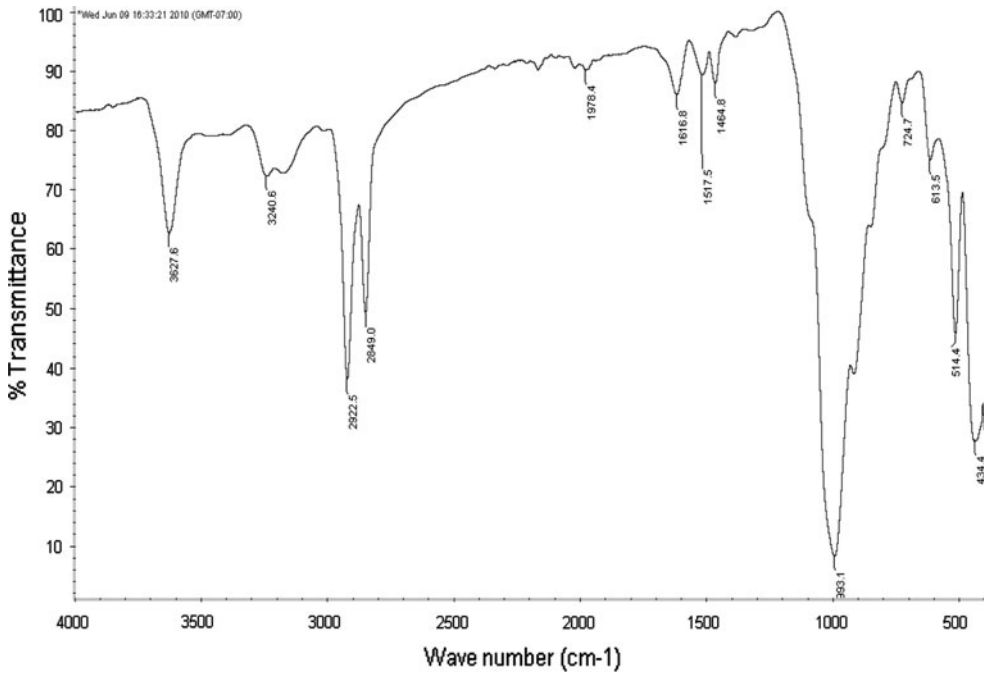

Fig. 5 FTIR spectrum of O-MMT

Table 3 Infrared absorption bands of the organoclay

Observed band (cm^{-1})	Band assignment	Ref.
3627.6	Al–O–H str	[25]
3240.6	Si–OH str	[25]
2849 & 2922	C–H str of CH_2 (from the modifier)	[26]
1616.8	O–H bending	[26]
1517.5 and 1464.8	N^+–H bending	[26]
993.1	Si–O str	[25]
724.7	CH_2 rocking (from the modifier)	[26]
514.4	Al–O–Si str	[25]
434.4	Si–O–Si str	[25]

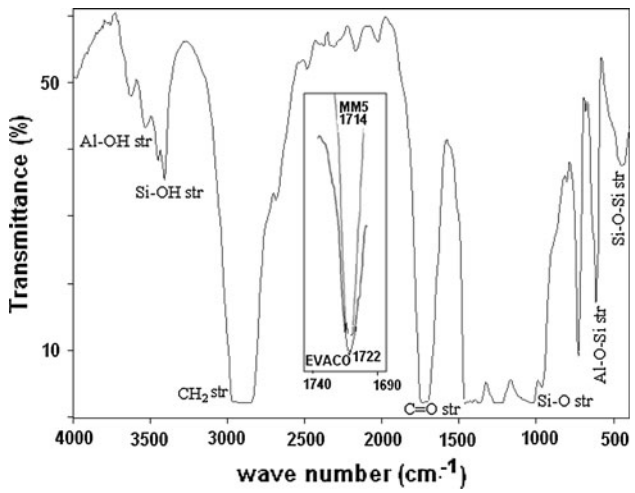

Fig. 6 FTIR spectrum of MM5 (the C=O stretching peaks of MM5 and EVACO have been highlighted in the insert)

The free energy change of the O-MMT/EVACO hybrid after mixing the clay in EVACO may be given as

$$\Delta G_P = \Delta H_P - T\Delta S_P \quad (2)$$

$$\Delta G_C = \Delta H_C - T\Delta S_C \quad (3)$$

Therefore, total free energy change of the system is

$$\Delta G_S = \Delta H_S - T\Delta S_S = \Delta H_S - T(\Delta S_P + \Delta S_C) \quad (4)$$

The subscripts P, C, and S, respectively in Eqs. 2–4 refer to the thermodynamic parameters of the pristine EVACO, O-MMT, and the hybrid, respectively.

ΔG_S value will be negative, and hence the most favorable interaction between the clay and the polymer will take place when ΔH_S is negative and ΔS_S is positive. When polymer chains enter into the gallery of the clay, they reside in a restrained form, i.e., ΔS_P is negative. In contrast, the expansion of the gallery by polymer chains causes the entropy change in the clay, ΔS_C, to be positive. If the clay layers are exfoliated, this may probably compensate the entropy loss associated with the confinement of polymer chains. Hence, in this condition, negative ΔH_S value makes

Table 4 T_g values of the EVACO/organoclay hybrids

Sample type	T_g
Control	−31.43 °C
MM1	−30.61 °C
MM3	−30.27 °C
MM5	−30.02 °C

ΔG_S negative. As a result, the mixing of the O-MMT with the EVACO will be thermodynamically favorable.

From Fig. 6, it can be seen that C=O peak position in neat EVACO is 1722 cm^{-1}, whereas the same in EVACO/O-MMT hybrid MM5 is 1714 cm^{-1} (the shift in wave number is due to intermolecular H-bonding between the Si–OH groups of O-MMT and C=O groups of EVACO). The ΔH of interaction between EVACO and O-MMT was found to be −1.89 kcal mol^{-1} ($\Delta H = 0.236\times -8 = -1.89$ kcal mol^{-1}), indicating that the interaction between O-MMT and EVACO is thermodynamically favorable.

DSC results

The DSC thermograms of pristine EVACO and the hybrids are shown in Fig. 7a and the T_g values are shown in Table 4. The increase in T_g of EVACO by the incorporation of clay (Fig. 7b) resulted from the restricted segmental motion of the polymer chains at the organic–inorganic interface, because of the confinement of the polymer chains at the clay layers. It was also reported in the literature that the majority of the other well-dispersed polymer nanocomposites also exhibited higher T_g than their corresponding pristine polymers.

In DSC thermograms of the nanocomposites (Fig. 7a), two endothermic peaks are observed. The presence of two peaks could be due to two reasons:

1. When a sufficiently large crystal is created by reorganization.
2. When different-sized crystals are present from the start.

The first peak refers to the melting of the fine crystallites, and the second peak refers to the melting of the bigger crystallites [29]. The second peak of the hybrids diminishes with increased clay loading, which might be because of the hindrance to crystallization of EVACO by O-MMT. Similar trend was reported earlier by some researchers [10–13] for some polymer–clay hybrids whose optical transparencies were enhanced by the well-dispersed nanoclay platelets suppressing polymer crystallization.

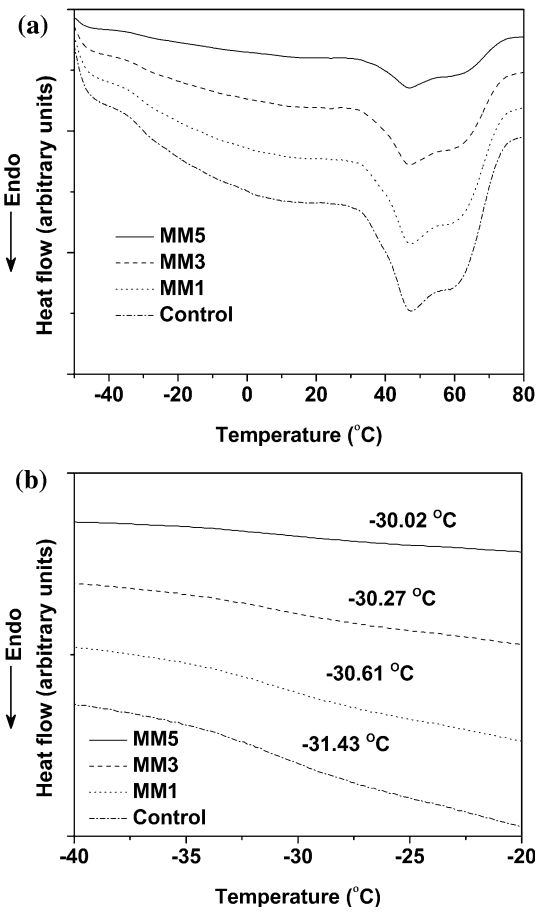

Fig. 7 **a** DSC traces of O-MMT/EVACO hybrids and **b** T_g transition of the O-MMT/EVACO hybrids from DSC

Mechanical properties

The mechanical properties of the EVACO/O-MMT hybrids are shown in Table 5 (along with standard deviations of the respective parameters), and the tensile force versus extension curves are shown in Fig. 8. The samples exhibit plastic deformation indicating the rubbery behavior of the EVACO and its O-MMT hybrids. It can be seen that the tensile strength and Young's modulus of the hybrids increase marginally up to a clay loading of 3%; while shore-A hardness and stresses at 100 and 300% strain of the hybrids increase as a function of clay loading, elongation at break decreases as a function of clay loading. The reduction of elongation at break is due to the restriction of polymer chain slippage due to their strong interaction with the clay layers. The FTIR spectroscopy results also support this observation. Within the selected experimental window, 3% clay loading gives the best balance of properties. The area under the load versus extension curve is a measure of toughness of the hybrids. It can be seen from Fig. 8 that the toughness as indicated by the area under the load versus extension curves decreases as the clay loading is increased. A similar trend has been reported for some polymer/MMT hybrid systems [30, 31].

Conclusions

XRD results reveal the predominance of intercalated morphology as the clay loading of the nanocomposites is increased. TEM exhibits the co-existence of exfoliated and intercalated morphologies for the current nanocomposite

Table 5 Mechanical properties of the EVACO/organoclay hybrids

Sample ID	Tensile strength (MPa)	Elongation @ break (%)	Young's modulus (MPa)	Stress at 100% strain (MPa)	Stress at 300% strain (MPa)	Hardness (Shore-A)
Control	4.0 ± 0.2	1435 ± 70	3.8 ± 0.1	1.8 ± 0.1	2.4 ± 0.2	70 ± 1
MM1	4.5 ± 0.3	1312 ± 40	4.1 ± 0.2	1.9 ± 0.1	2.4 ± 0.3	74 ± 1
MM3	4.6 ± 0.2	1235 ± 35	4.2 ± 0.1	2.0 ± 0.2	2.4 ± 0.3	79 ± 2
MM5	3.9 ± 0.3	1165 ± 34	3.6 ± 0.2	2.3 ± 0.2	2.7 ± 0.2	85 ± 2

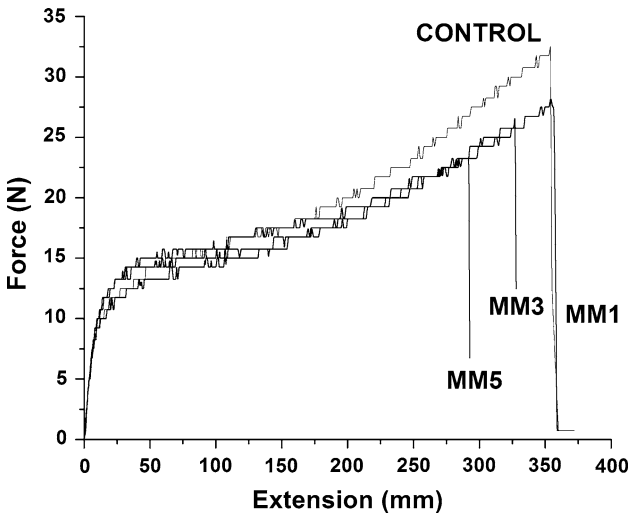

Fig. 8 Tensile force versus extension curves of O-MMT/EVACO hybrids

systems at all levels of clay loading. EVACO and O-MMT interact with each other in a thermodynamically favorable manner, and this strong interaction hinders crystallization of EVACO. The organically modified nanoclay distributes and disperses well in EVACO matrix as evidenced by EDX results; this along with the good polymer-clay interaction lead to an increase in tensile strength, Young's modulus, and shore-A hardness of the hybrids up to a clay loading of 3%. Beyond this loading, the tensile strength and Young's moduli deteriorate. Among the three EVACO/O-MMT hybrids studied, 3% of clay loading seems to impart the optimum balance of mechanical properties.

Acknowledgments One of the authors, SA, gratefully acknowledges the funding through seed money grant (2009–2011) by the National Institute of Technology Karnataka, India.

References

1. Krummenacker M, Lewis J (eds) (1995) Prospects in nanotechnology toward molecular manufacturing. John Wiley, New York
2. Bhushan B (ed) (2004) Springer handbook of nanotechnology. Springer, Berlin
3. NASA Science (2010) Science news: audacious and outrageous: space elevators. http://science.nasa.gov/headlines/y2000/ast07sep_1.htm. Accessed Dec 2010
4. Luther W, Bachmann G (Eds) (2008) Nanoparticles-small thing, big effects; german federal ministry of education and research, division of nanomaterials, new materials. http://www.bmbf.de/pub/nanoparticles_small_things_big_effects.pdf. Accessed Dec 2010
5. Fendler JH (ed) (1998) Nanoparticles and nanostructured films: preparation, characterization and applications. Wiley-VCH, Weinheim
6. Ray SS, Okamato M (2003) Prog Polym Sci 28:1539
7. Alexandre M, Dubois P (2000) Mater Sci Eng 28:1
8. Ding C, Jia D, He H, Guo B, Hong H (2005) Polym Testing 24:94
9. Camargo PH C, Satyanarayana KG, Wypych F (2009) Mater Res 12:1
10. Giannelis EP (1996) Adv Mater 8:29
11. Vaia RA, Jandt KD, Kramer E, Giannelis EP (1996) Chem Mater 8:2628
12. LeBaron PC, Wang Z, Pinnavaia T (1999) J Appl Clay Sci 15:11
13. Morgan AB (2007) Mater Matters 2:20
14. Giese RF, Van Oss CJ (2002) Colloid and surface properties of clays and related minerals. Marcel Dekker, New York
15. Ma X, Lu H, Liang G, Yan H (2004) J Appl Polym Sci 93:608
16. Blumstein A (1965) J Polym Sci A 3:2665
17. Theng BKG (1979) Formation, properties of clay–polymer complexes. Elsevier, Amsterdam
18. Vaia RA, Ishii H, Giannelis EP (1993) Chem Mater 5:1694
19. Clarence V (1979) US Patent 4137382
20. Hoh G (1979) US Patent 4172939
21. Emslander OJ (2010) US Patent 6316120
22. Srivatsan N, Mallya P, Holguin DL, Wouters D, Bartholomew EL, Lofton LP (2010) US patent 2010/0266837 A1
23. Klee D, Höcker H (1999) Adv Polym Sci 149:1
24. Audic JL, Reyx D, Brosse JC (2003) J Appl Polym Sci 89:1291
25. Nayak PS, Singh BK (2007) Bull Mater Sci 30:235
26. Smith B (1999) Infrared spectral interpretation—a systematic approach. CRC press, Boca Raton
27. Kader MA, Bhowmick AK (2003) Polym Degrad Stab 79:283
28. Maiti M, Bhowmick AK (2006) J Polym Sci B Polym Phys 44:162
29. Tsuchiya M, Kojima T (2005) J Therm Anal Calor 80:159
30. Cho JW, Paul DR (2001) Polymer 42:1083
31. Fornes TD, Yoon PJ, Keskkula H, Paul DR (2001) Polymer 42:9929